Macromolecules
ARTICLE

Macromolecules **2010**, *43*, 10679–10691 **10679**
DOI: 10.1021/ma1019945

Effect of Solvent Quality on the Coil−Stretch Transition

Shikha Somani

Department of Chemical Engineering, Stanford University, Stanford, California 94305, United States

Eric S. G. Shaqfeh*

Departments of Chemical and Mechanical Engineering, Stanford University, Stanford, California 94305, United States

J. Ravi Prakash

Department of Chemical Engineering, Monash University, Clayton, VIC 3800, Australia

Received August 31, 2010; Revised Manuscript Received November 11, 2010

ABSTRACT: Polymers undergo a sharp coil−stretch transition in extension dominated flows when the strain rate exceeds a critical strain rate. We investigate this transition in both Θ solvents and good solvents using Brownian dynamics simulations. The polymer is represented by a bead−spring chain model undergoing elongational flow and solvent-mediated effects such as fluctuating hydrodynamic interactions (HI) and excluded volume (EV) are included rigorously. A 1-D energy landscape theory with an activation energy for transition[1] is used to gain qualitative insights into the dynamics. A key factor in determining the influence of solvent quality is the use of a proper measure of solvent quality.[2,3] Contrary to earlier findings, it is observed that with improvement in solvent quality, the critical strain rate at which the coil to stretch transition takes place decreases. Furthermore, the solvent quality has a profound effect on the scaling of the critical strain rate with molecular weight and on both the transient and steady state properties of the system. Universal functions are shown to exist for the observed dynamic and static properties, which will prove useful in determining the operating parameters for experiments.

1. Introduction

In fluid mechanics, transitions are generally associated with peculiar dynamics. It is well-known that addition of a minute amount (of the order of parts per million) of high molecular weight polymers to a solvent can engender remarkable non-Newtonian flow behavior like turbulent drag reduction and dramatic flow thickening beyond a critical strain rate in porous media flows. Such phenomena have tremendous commercial importance and have been attributed to the most fundamental properties of a polymer—extensibility and orientability. In particular, in stretching flows (extension dominated flows), a transition from an ambient coiled state to a stretched conformation (known as the coil−stretch transition) is known to modify flow behavior dramatically. Extensional flows are of considerable importance and occur in flows through orifices, filters, porous media, constrictions in pipes and in any turbulent flow. In fact, most practical flow systems contain an extensional component.

There has been controversy over the dynamics surrounding the polymer coil stretch transition over many years. The debate finds its origin in the first order coil−stretch transition proposed by de Gennes in his seminal paper in 1974.[4] De Gennes envisaged polymer conformations tracing an S-shaped curve as a function of strain rate leading to coil−stretch hysteresis in stretching flows. Similar ideas were advanced in the same year by Hinch[5] and a year later by Tanner.[6] During the era from 1974 to 2003, the scientific community was divided over the existence of coil−stretch hysteresis. The S-shaped curve was considered an artifact of mathematical approximations by many scientists.[7−9] Using a bead−spring chain instead of a dumbbell model for small polymer chains, a gradual transition from the coiled equilibrium chain to the stretched state was observed without any hysteresis.[8] A stochastic approach as a basis for Brownian dynamics simulation for a freely jointed bead-rod chain, with constant hydrodynamic interaction also did not show hysteresis.[9]

In contrast, simulation of the motion of a dumbbell with a conformation dependent friction coefficient, using the Brownian dynamics technique, resulted in an S-shaped curve (hysteresis).[10] A nonlinear dumbbell with varying friction coefficient on extension without the Peterlin approximation also showed hysteresis.[11] A computational scheme with conformation dependent hydrodynamic interaction also predicted coil-stretch transition in steady elongational flow, with hysteresis in the value of the extensional viscosity.[12] When the extensional viscosity was modeled for a FENE dumbbell with and without a conformation dependent friction, hysteresis was observed only with conformation dependent drag.[13]

The controversy was resolved by single molecule experiments and Brownian dynamics simulations in 2003.[1] *Escherichia coli* DNA molecules (1.3 mm) were observed to coexist in two different conformations (depending on their initial conformation) at the same strain-rate for a long time. Birefringent pipes, observed in the experiments earlier,[14] could therefore be safely assumed to be manifestations of the hysteresis phenomenon.[15] Stress measurements using the filament stretching rheometer have since also demonstrated the physical implications of hysteresis phenomenon on bulk properties.[16]

*Corresponding author. E-mail: esgs@stanford.edu.

Published on Web 12/01/2010

The comprehensive picture that has now emerged from these earlier studies is as follows: There are three conditions that should be met for a polymer to undergo a coil to stretch transition. First, the flow should be extensionally dominated for sharp coil−stretch transitions. Second, the strain rate should be sufficiently high so that the drag force can overcome the entropic force. Third, the polymer should experience the high strain rate for a sufficiently long time for the given fluid to attain the required strain. In systems with a stagnation point, the fluid lines near the center line are subject to the very high strains necessary for the coiled polymers to extend. The coil−stretch transitions are known to be accompanied by a significant slowdown in polymer dynamics in elongation flows, and there have been several interesting studies exploring the nature of this transition as a function of flow type and chain length.[17,18]

Regarding coil−stretch hysteresis, the present picture that has emerged unifies all previous observations. It undoubtedly supports the previous work by Hinch,[5] Tanner,[6] Brestkin,[11] Magda et al.,[12] Darinskii et al.,[10] and others that hysteresis exists and has implications on macroscopic properties of polymer solutions.[19] On the other hand, the present theory also explains why some researchers[7−9] could not find hysteresis in their systems. As postulated by the earlier careful mathematical analysis[7] there exists a unique probability distribution at infinite time. Hysteresis is a transient phenomena due to kinetically trapped molecules in different conformations depending on their previous history and accordingly hysteresis vanishes at steady state.[7] Also, for hysteresis to be observed the difference in the drag in the coiled and stretched states should be sufficiently large ($\xi_{stretched}/\xi_{coiled} \geq 4.5$).[1,20,21] This condition is satisfied only for long chains and hence hysteresis is not observed in short chains[8] or for chains without a conformation dependent drag.[9]

Existence of hysteresis can be understood with an analogy to an energy landscape with an activation barrier.[21] There is one global minima of the system and hence one steady state. However the chains are kinetically trapped in two wells separated by the activation barrier and depending on the initial conformation of the polymer, the polymer lies preferentially in one of the two wells at some finite time.[21] The rate of hopping from one well to the other is affected by various parameters of the system which include the length of the polymer[22] and the mixedness in planar flows.[23] Even though the controversy surrounding the existence of hysteresis has been removed, our present understanding is still limited to ideal solvents. There are still controversial results surrounding the effect of solvent quality on the coil stretch transition and hence hysteresis.

There have been several attempts in the past to study the effect of solvent quality on the coil stretch transition.[14,24−27] Experimentally, the coil stretch transition has been followed by measuring the birefringent intensity against strain rate in a well-defined extensional flow field. The experimental studies suffer from several inherent drawbacks. First, polydispersity is a very important issue as the critical strain rate is very sensitive to the molecular weight of the polymer. As has been clearly pointed out by many experimentalists,[25] the molecular size value (N) provided by commercial suppliers has substantial errors especially for large molecular weight polymers and hence it is difficult to get monodisperse samples for accurate experimental studies. Second, the experimental set-ups used are characterized by a number of issues. In the opposed jets device,[28] the jets offer very high strain rates at low Reynolds number with relative freedom from wall effects, but the cylindrical symmetry makes the detailed assessment of the birefringence problematic. In the cross slot device, birefringence measurements are easy, but the effects of walls are likely to be pronounced. In the four-roll mill, the developed flow field has a more uniform strain rate throughout, than for both the jets and the cross-slots (which contain stationary surfaces and sharp corners at the edge of the flow).[29] However, turbulence sets in at high velocity gradients and therefore the mill tends to be useful only for low strain rate work.[14,29] Apart from these, experiments also suffer from rather limited residence time near the stagnation point and contribution of solvent orientation to the solution's optical anisotropy.

Given these inherent limitations, it is not surprising that some researchers[14,24−27] have found the scaling exponent of the critical strain rate with molecular weight to be independent of the solvent quality (−1.5 for both Θ and good solvents), while others[30,31] have found the exponent to be a function of solvent quality. Discrepancy in these experiments[14,24,25,27] can be attributed to the use of various polymer−solvent combinations to change the solvent quality, leading to some hitherto unknown specific polymer−solvent interaction or possible differences in polymer−solvent chemistry.[26] It is relevant in this context to point out that even with experiments with the same polymer solvent system but varying the temperature to change the solvent quality, mixed results have been obtained: −1.5 and −1.8.[26,31]

Because of the inherent limitations of the experimental techniques, some researchers have used theoretical[32] and computational methods like Monte Carlo[33,34] and Brownian dynamic simulations[35] to explore the effect of solvent quality on the coil stretch transition. However their results are also contradictory and cover a wide range of the scaling exponents from −2.3 to −1.5.[33,35] Apart from the effect of solvent quality on the scaling exponent, its effect on the absolute value of the critical strain rate is also widely debated with a few reporting it to be unaffected,[35] while most others found it to decrease with solvent quality irrespective of its effect on the scaling exponent.[14,26,31,34,36] The present work aims at resolving both these issues and gain more insight into the coil−stretch transition phenomenon using Brownian dynamics simulations. Almost all earlier studies have assumed that holding temperature constant keeps the solvent quality fixed, without accounting for the effect of molecular weight on solvent quality. We believe this is responsible for the mixed results observed for the effect of solvent quality on scaling exponent. In this work, a solvent quality measure is used, that captures the effect of molecular weight as well as temperature. Using extrapolation techniques, steady state and universal properties are also explored.

This article is organized as follows. Various physical forces and their corresponding models and parameters with the governing equations for polymer dynamics are discussed in section 2. In section 3, we first perform theoretical analysis using a dumbbell model to explore the important qualitative aspects of the coil to stretch transition and hysteresis in Hookean chains. In section 4, two different relaxation times are computed and the universal function of their ratio is examined. In section 5, qualitative and quantitative aspects of coil stretch transitions are explored in three different ways based on the different aspects of polymer dynamics. In section 6, results including the scaling exponent with molecular weight and various universal properties are discussed. The main conclusions of this study are summarized in section 7.

2. Simulation Methodology

To simulate complex fluids, the Brownian dynamics simulation technique is appropriate because of the different time scales involved.[37,38] In Brownian dynamics, the solvent is often treated as a continuum and the long, linear, flexible polymer is represented by a multi bead−spring chain with N beads connected by $(N - 1)$ massless springs. The overall drag coefficient of a bead (submolecule) is assumed to be a constant ζ_0. Any submolecule resists separation of its ends due to entropic considerations and this is captured in the "spring" of the bead−spring model. The insertion of N spherical beads of radius $a = \zeta_0/(6\pi\eta_s)$ between

adjacent springs (including beads at the chain ends) then completes the mechanical representation of the molecule as a bead spring chain. Here η_s is the solvent viscosity. Thus, the beads act as centers of hydrodynamic resistance while the springs account for the entropic force between two beads.[39]

Apart from the entropic force of springs along the polymer chain backbone, there are four different forces that act on the polymer due to the solvent. Drag force acts due to the relative motion between polymer segment and solvent molecules moving under the influence of an externally imposed velocity field. In addition to these, polymer chains also experience Brownian forces due to the thermal motion of the solvent molecules. Moreover, there are two long-range solvent-mediated interactions between parts of the polymer segments that are far apart along the chain. These are the excluded volume and hydrodynamic interactions. Excluded volume interactions arise due to the fact that no two parts of a polymer molecule can occupy the same space at the same time i.e. the polymer segments cannot physically overlap. Hydrodynamic interactions arise due to the perturbation of the velocity field around a polymer segment due to the motion of all the other segments of the polymer. Brownian forces and excluded volume interactions affect both the equilibrium and nonequilibrium properties of the polymeric solution while the drag force and hydrodynamic interactions affect only the dynamic properties.

In general, two equivalent approaches are possible for an accurate quantitative description of the dynamics of a system of Brownian particles: solution of the phase space (configuration space) distribution of particle position via a Fokker−Planck equation or direct simulation of particle trajectories with a Langevin description of particle motion, from which the appropriate distribution functions may be calculated.

Using polymer kinetic theory and stochastic calculus, the Fokker−Planck equation for the evolution of configurational probability distribution $\Psi(r_1,r_2,...,r_N)$ is given by[39]

$$\frac{\partial \Psi}{\partial t} = -\sum_{i=1}^{N} \frac{\partial}{\partial r_i} \cdot \left\{ \kappa \cdot r_i + \frac{1}{\zeta_0} \sum_{j=1}^{N} \gamma_{ij} \cdot F_j^{\phi} \right\} \Psi + \frac{k_B T}{\zeta_0} \sum_{i,j=1}^{N} \frac{\partial}{\partial r_i} \cdot \gamma_{ij} \cdot \frac{\partial \Psi}{\partial r_j} \tag{1}$$

where k_B is the Boltzmann constant, T is the absolute temperature of the solution and κ is the transpose of the position-independent velocity gradient ∇v. For spatially homogeneous flows, the velocity field of this solvent continuum can be expressed as $v = v_0 + \kappa \cdot r$, where v_0 is the constant velocity of the reference frame and r is the position vector of any point with respect to the origin of the frame of reference. In this work, we explore planar extensional flows for which the coil stretch transitions are very sharp and the velocity gradient is given by:

$$\kappa = \dot{\varepsilon} \begin{pmatrix} 1 & 0 & 0 \\ 0 & -1 & 0 \\ 0 & 0 & 0 \end{pmatrix} \tag{2}$$

where $\dot{\varepsilon}$ is the strain rate for the extensional flow. γ_{ij} are the diffusion tensors that are related to the hydrodynamic interaction tensors described later. F_j^{ϕ} represents the total force on a bead j due to nonhydrodynamic conservative intramolecular interactions. The nondimensional Ito stochastic differential equation (Langevin equation) corresponding to the Fokker−Planck equation shown above is given by a force balance for each bead:

$$dr_i^* = \left(\kappa_{ij} \cdot r_j^* + \frac{1}{4} \sum_k D_{ik}^* \cdot (F_k^{*s} + F_k^{*E}) \right) \mathrm{d}t^* + \frac{1}{\sqrt{2}} \sum_k B_{ik}^* \, \mathrm{d}W_k^* \tag{3}$$

The characteristic length and time scales used for nondimensionalization are

$$l_H = \sqrt{\frac{k_B T}{H}}$$

and

$$\lambda_H = \frac{\zeta_0}{4H}$$

respectively, where ζ_0 is the bead friction coefficient and H is the Hookean spring constant. $\boldsymbol{D}_{ik}^*$ is the mobility tensor that captures the hydrodynamic interaction between different segments of the polymer. There are many possible choices for the mobility tensor and we choose $\boldsymbol{D}_{ik}^*$ as the Rotne−Prager−Yamakawa (RPY) tensor[21,40] since it is positive-semidefinite for all polymer chain configurations. It is given by

$$\boldsymbol{D}_{ij}^* = \begin{cases} \delta_{ij} & \text{if } i = j \\ \dfrac{3\sqrt{\pi}}{4} \dfrac{h^*}{r_{ij}^*} \left[\left(1 + \dfrac{2\pi}{3} \dfrac{h^{*2}}{r_{ij}^{*2}} \right) \delta_{ij} + \left(1 - 2\pi \dfrac{h^{*2}}{r_{ij}^{*2}} \right) \dfrac{r_{ij}^* r_{ij}^*}{r_{ij}^{*2}} \right] & \text{if } i \neq j \text{ and } r_{ij}^* \geq 2\sqrt{\pi} h^* \\ \left[\left(1 - \dfrac{9}{32\sqrt{\pi}} \dfrac{r_{ij}^*}{h^*} \right) \delta_{ij} + \dfrac{3}{32\sqrt{\pi}} \dfrac{1}{h^*} \dfrac{r_{ij}^* r_{ij}^*}{r_{ij}^*} \right] & \text{if } i \neq j \text{ and } r_{ij}^* < 2\sqrt{\pi} h^* \end{cases} \tag{4}$$

where r_{ij} is the vector between beads i and j and h^* is the hydrodynamic interaction parameter defined as

$$h^* = a \sqrt{\frac{H}{\pi k_B T}}$$

The parameter a is the bead radius such that $6\pi\eta_s a = \zeta_0$. The quantity h^* is the approximate ratio of the bead radius to the equilibrium extension of a spring; hence physically acceptable values of h^* are less than 0.5. Specifically we choose $h^* = 0.24$ which corresponds to the fixed point value for h^* at which the properties reach universal values at smaller values of number of beads.[41]

Using the fluctuation−dissipation theorem, the matrix $\boldsymbol{B}_{ik}^*$ representing the strength of fluctuations in the system is related to the diffusion matrix $\boldsymbol{D}_{ij}^*$ which characterizes the dissipative processes in the system as follows[21,40]

$$\boldsymbol{B}_{ik}^* \boldsymbol{B}_{jk}^* = \boldsymbol{D}_{ij}^* \tag{5}$$

The differential equation is solved using the two-step predictor corrector method.[42−44] The computational intensity of the decomposition of the diffusion matrix $\boldsymbol{D}_{ij}^*$ into the coefficient tensor $\boldsymbol{B}_{ik}^*$ scales as N^3 when Cholesky decomposition is used. However when Fixman's idea of treating the product of the coefficient matrix with the Weiner process vector as one element is implemented with the Chebyshev polynomial approximation, the cost of the calculation is considerably reduced. Hence we have used Fixman's method in our computations and the details of the exact algorithm can be found elsewhere.[2]

$\boldsymbol{F}_k^{*s}$ is the entropic spring force and we use Hookean chains. $\boldsymbol{F}_k^{*E}$ is the excluded volume force and it ensures that the polymer segments do not physically overlap. Since there are only two entities with which a polymer can interact—polymer or solvent—introducing repulsion between polymer segments indirectly imposes a favorable interaction between polymer and solvent leading to an improvement in solvent quality. The EV repulsive potential between two beads is given by[45]

$$\phi^e = -\frac{\nu k_B T}{(2\pi)^{3/2} d^3} \, \mathrm{e}^{-r^2/2d^2} \tag{6}$$

and the corresponding EV force between two beads is given by

$$\boldsymbol{F}^{*E}(r) = \frac{\partial \phi^e}{\partial r} = \frac{\nu k_B T}{(2\pi)^{3/2} d^5} e^{-r^2/2d^2} r \quad (7)$$

where the EV parameter ν quantifies the strength of the EV potential, d is the spatial range of the potential, and r is the distance between two beads. This form of EV potential has been validated under various equilibrium and nonequilibrium conditions,[41,46−49] showing that this potential effectively captures the EV effect. It approaches the ideal δ-form of the potential as d approaches zero. Being a smooth potential, it does not require extremely small timesteps for accurate computations as otherwise needed for the Lennard-Jones (LJ) potential. The connection between the experimental and theoretical definition of solvent quality z is given by[41]

$$z = \nu_0(1 - T_\theta/T)\sqrt{M} = \nu\left(\frac{H}{2\pi k_B T}\right)^{3/2}\sqrt{N} = z^*\sqrt{N} \quad (8)$$

where ν_0 is a chemistry dependent constant, T_θ is the Θ-temperature and z^* is the strength of the EV potential. Perturbation analysis of the equilibrium properties in the strength of excluded volume interaction z^* establishes that the true perturbation parameter is $z = z^*\sqrt{N}$.[50] Furthermore, it has been largely substantiated by various experimental results wherein a variety of polymer-solvent systems, when plotted as a function of z, have been shown to display universal behavior (even at temperatures well above the Θ temperature).[50] With the narrow Gaussian potential (eq 6), the solvent quality can be modified by varying a single parameter z unlike the involved procedure of evaluating two parameters in the LJ potential to get any desired solvent quality.[51,52] From eq 8, solvent quality can be varied experimentally by either varying the solvent−polymer combination or by changing the temperature of the solution or by changing the molecular weight of the polymer. In most experimental investigations of the solvent quality effect, the solvent quality was varied by changing the solvent−polymer combinations,[14,24,25,27] and in some cases by keeping the solvent−polymer combination the same but varying the temperature of the solution.[26,31] However it is important to note that when the molecular weight is varied to calculate the scaling exponent holding ν_0 and T constant, the solvent quality changes. Also, in almost all of the previous computational studies, temperature, i.e. parameters equivalent to z^*, were assumed to be constant in order to keep the solvent quality fixed.[35] In such cases when the molecular weight of the polymer is changed to evaluate the scaling of the critical strain rate with polymer size, the solvent quality changes. Hence the scaling exponent (with molecular weight) is not evaluated at a fixed solvent quality as desired. We hold the solvent quality measure z constant to keep the solvent quality fixed and vary z^* to compensate any change induced by a variation in polymer molecular weight (N).

It is also worthwhile here to discuss briefly our assumption of a Hookean spring force law. Since we are interested in the influence of solvent quality, at first sight it would appear to be more appropriate to use the nonlinear Pincus force law, $F \sim R^{3/2}$ as the appropriate description of the force−extension behavior for intermediate extensions. However, this force law describes the large length scale deformation of the end-to-end vector R of a polymer chain in a good solvent, and not the deformation at the segmental level. As is well-known, the Pincus force law can be derived by a simple scaling argument using the concept of "tension" blobs [see ref 53, pp 104−107], where the blob represents the length scale at which the stretching energy becomes of order k_BT. At length scales smaller than the blob size, the thermal energy randomizes the configurations of the chain, and the chain remains in its unperturbed swollen state. At larger length scales, the chain is stretched into a linear sequence of aligned tensile blobs. It is the existence of chain connectivity and excluded volume interactions between segments that leads to the nonlinear force−extension behavior of the end-to-end vector. Any simulation that includes these aspects in a coarse-grained model inevitably obeys the Pincus force law at large length scales. Essentially, the Pincus force law is a *consequence* of these physical phenomena, and does not have to be put in by hand. It must be noted, however, that sufficient number of degrees of freedom must be included in the model for the Pincus force law to be manifested. If a highly coarse-grained model is used to represent a polymer chain in a good solvent, then using a Pincus force law for a spring is a way of capturing the self-similar behavior of a large segment of the chain at the level of a single spring. Note that the spring force law can be written in the general form $F = R^{\nu/(1/\nu)}$ such that the Hookean force law is recovered for $\nu = {}^1/_2$ in a Θ-solvent, and the Pincus force law is recovered for $\nu = {}^3/_5$ in a very good solvent. These power-law exponents are only valid in these limits, and the use of a force-law with an *effective* exponent ν in the *crossover* region between the limits of Θ and good solvent is not a valid procedure. In order to understand the crossover regime in the context of the blob anstaz requires the use of a subtle scaling argument involving *two* blob length scales—a *thermal* blob length scale and a *tensile* blob length scale. An example of the use of a two-blob scaling argument can be found in ref 53 (see Figure 5.5, p 178), in the context of chain configurations in semidilute solutions. The correct nonlinear force in the crossover regime (which interpolates between the two limits of Hookean and Pincus force laws) will automatically be captured in our simulations since we have carried them out at constant values of z, and have incorporated chain connectivity and excluded volume interactions in our coarse-grained model. This is borne out by the quantitative agreement seen previously between experimental observations and Brownian dynamics simulations of the conformational evolution, and extensional viscosity of DNA solutions, when a similar procedure was followed for simulating the crossover regime[41,48]

3. 1-D Energy Landscape Theory

Before carrying out the rigorous Brownian dynamic simulations, we explore the effect of solvent quality using a 1-D theory based on a toy dumbbell model. In a dumbbell model, the polymer is represented by two beads connected by a spring. The Fokker−Planck equation for a dumbbell projected in 1-D is then given by

$$\frac{\partial \psi}{\partial t} = -\frac{\partial}{\partial Q}\cdot\left[\left\{\kappa\cdot Q - 2\frac{H_{DB}Q}{\zeta(Q)}\right\}\psi - \frac{2k_BT}{\zeta(Q)}\frac{\partial \psi}{\partial Q}\right] \quad (9)$$

where Q is the distance between the two end beads which captures the transformation from coiled to stretched state and H_{DB} is the Hookean spring constant for a dumbbell. The hydrodynamic interactions are incorporated by introducing a conformation dependent drag coefficient $\zeta(Q)$ as postulated by DeGennes.[4] $\zeta(Q)$ represents the average drag coefficient over all possible conformations with Q as the end-to-end extension. This simple heuristic assumption was later supported with the rigorous evaluation of the exact functionality of $\zeta(Q)$ for a dumbbell using multibead−spring simulations.[22] We nondimensionalize this equation with the characteristic time

$$\lambda_H = \frac{\zeta_0}{4H_s}$$

and length scale

$$l_H = \sqrt{\frac{k_BT}{H_s}}$$

where ζ_0 is the bead friction coefficient and $H_s = NH_{DB}$ is the Hookean spring constant for a single spring in the multibead-chain representation of the polymer. Using

$$g(Q^*) = \frac{\zeta(Q^*)}{\zeta_0}$$

the nondimensional form of the equation is given by

$$\frac{\partial \psi}{\partial t^*} = -\frac{\partial}{\partial Q^*}\cdot\left[\left(PeQ^* - \frac{1}{N}\frac{1}{g(Q^*)}Q^*\right)\psi - \frac{1}{2}\frac{1}{g(Q^*)}\frac{\partial \psi}{\partial Q^*}\right] \quad (10)$$

where

$$Pe = \frac{\dot{\varepsilon}\zeta_0}{4H_s}$$

is the dimensionless strain rate. At steady state,

$$\frac{\partial \psi}{\partial t^*} = 0$$

and the solution is given by

$$\psi = \psi_0 \exp\left(-\int_0^{Q^*}\left(\frac{1}{N} - 2(Pe)g(q)\right)q\,\mathrm{d}q\right) \quad (11)$$

The argument of the exponential can be thought of as the "conformational energy" of the dumbbell[21] such that

$$\frac{E(Q^*)}{k_B T} = \int_0^{Q^*}\left(\frac{1}{N} - 2(Pe)g(q)\right)q\,\mathrm{d}q \quad (12)$$

One of the peculiar properties of a Hookean chain is that it can extend unboundedly. The hydrodynamic interactions between different parts of the chain vanish after the chain extends to a significant extent as the parts are separated by physical distances too large to be influenced by the motion of other parts. Hence it is safe to assume that there exists some Q_0^* such that for $Q^* < Q_0^*$, there is hydrodynamic interaction between parts of the chain, however for $Q^* \geq Q_0^*$, the chain shows more Rouse like behavior such that

$$g(Q^*) = \frac{\zeta(Q^*)}{\zeta_0} = \begin{cases} \zeta_c^* + \zeta_c^*\left(\dfrac{\zeta_s^*}{\zeta_c^*} - 1\right)\dfrac{Q^*}{Q_0^*} & \text{if } Q^* < Q_0^* \\ \zeta_s^* & \text{if } Q^* \geq Q_0^* \end{cases} \quad (13)$$

where

$$\zeta_c^* = \frac{\zeta_{\mathrm{coil}}}{\zeta_0} \sim (\mathrm{Zimm}) \sim N^{\nu} \quad (14)$$

and ν is 0.5 in a θ solvent and 0.588 in a very good solvent.[54]

$$\zeta_s^* = \frac{\zeta_{\mathrm{stretched}}}{\zeta_0} \sim (\mathrm{Rouse}) \sim N \quad (15)$$

Hence, neglecting prefactors of order 1,

$$g(Q^*) = \begin{cases} N^{\nu}\left(1 + (N^{1-\nu} - 1)\dfrac{Q^*}{Q_0^*}\right) & \text{if } Q^* < Q_0^* \\ N & \text{if } Q^* \geq Q_0^* \end{cases} \quad (16)$$

The deterministic forces are then given by

$$F_{\mathrm{drag}}^* = \frac{F_{\mathrm{drag}}}{\sqrt{k_B T H_s}} = PeQ^* g(Q^*, N) \quad (17)$$

$$F_{\mathrm{sp}}^* = \frac{F_{\mathrm{sp}}}{\sqrt{k_B T H_s}} = \frac{H_{DB}Q}{\sqrt{k_B T H_s}} = \frac{H_{DB}}{H_s}\frac{Q}{\sqrt{k_B T/H_s}} = \frac{1}{N}Q^* \quad (18)$$

Since the intersection between the above two forces determines the maxima or minima in the corresponding energy landscape (see eq 12 and Figure 1), we define the difference slope S as

$$S = \frac{\mathrm{d}F_{\mathrm{drag}}^*}{\mathrm{d}Q^*} - \frac{\mathrm{d}F_{\mathrm{sp}}^*}{\mathrm{d}Q^*} = Pe\frac{\mathrm{d}}{\mathrm{d}Q^*}(Q^* g(Q^*)) - \frac{1}{N} \quad (19)$$

We consider the two regions separately: $0 < Q^* < Q_0^*$ and $Q^* \geq Q_0^*$.

1. For $Q^* \geq Q_0^*$, $F_{\mathrm{drag}}^* = PeQ^*N$ and $F_{\mathrm{sp}}^* = (1/N)Q^*$. There are three possibilities:

$$(F_{\mathrm{drag}}^* > F_{\mathrm{sp}}^*)|_{Q^* = Q_0^*} \Rightarrow (S|_{Q^* = Q_0^*} > 0)$$

$$\text{and} \quad (F_{\mathrm{drag}}^* > F_{\mathrm{sp}}^*)|_{Q^* > Q_0^*} \Rightarrow \text{no intersections (Figure 1e)}$$

$$(F_{\mathrm{drag}}^* = F_{sp}^*)|_{Q^* = Q_0^*} \Rightarrow (S|_{Q^* = Q_0^*} = 0)$$

$$\text{and} \quad (F_{\mathrm{drag}}^* = F_{\mathrm{sp}}^*)|_{Q^* > Q_0^*} \Rightarrow \text{lines are simply identical}$$

$$(F_{\mathrm{drag}}^* < F_{\mathrm{sp}}^*)|_{Q^* = Q_0^*} \Rightarrow (S|_{Q^* = Q_0^*} < 0)$$

$$\text{and} \quad (F_{\mathrm{drag}}^* < F_{\mathrm{sp}}^*)|_{Q^* > Q_0^*} \Rightarrow \text{no intersections (Figure 1a)}$$

2. For $0 \leq Q^* < Q_0^*$, there is one intersection at $Q^* = 0$, and to find other points of intersection, we consider the following cases:

$$S|_{Q^*=0} \geq 0 \Rightarrow (F_{\mathrm{drag}}^* > F_{\mathrm{sp}}^*)|_{Q^* = Q_0^*} \Rightarrow \text{no second intersection (Figure 1e)}$$

$$S|_{Q^*=0} < 0 \quad \text{and} \quad (F_{\mathrm{drag}}^* > F_{\mathrm{sp}}^*)|_{Q^* = Q_0^*} \Rightarrow \text{second intersection (Figure 1c)}$$

$$S|_{Q^*=0} < 0 \quad \text{and} \quad (F_{\mathrm{drag}}^* < F_{\mathrm{sp}}^*)|_{Q^* = Q_0^*} \Rightarrow \text{no second intersection (Figure 1a)}$$

Accordingly, we can demarcate the three different cases as shown in Figure 1 with the critical strain rates separating the three regions as

$$\underset{(100\%\ \mathrm{Coiled})}{\overset{Pe_{\mathrm{lower}}}{\longleftarrow}} \quad \underbrace{< \ Pe \ <}_{(\mathrm{Energy\ barrier})} \quad \underset{(100\%\ \mathrm{Stretched})}{\overset{Pe_{\mathrm{upper}}}{\longrightarrow}} \quad (20)$$

The chains do not hop when Pe is lower than the Pe_{lower} even if one waits for infinite strain while all chains hop for strain rates above Pe_{upper}. In between the two limits, one finds that some chains hop and some do not and this region corresponds to the hysteretic region and the energy landscape shows an activation barrier. These two limits are found to scale with molecular weight in Θ solvents as follows:

$$Pe_{\mathrm{upper}} : (S|_{Q^*=0}) = 0 \Rightarrow Pe_{\mathrm{upper}} \sim N^{-(1+\nu)}$$

$$Pe_{\mathrm{lower}} : F_{\mathrm{drag}}^*(Q_0^*) = F_{\mathrm{sp}}^*(Q_0^*) \Rightarrow Pe_{\mathrm{lower}} \sim N^{-2}$$

In conclusion, one can see that hysteresis occurs for Hookean chains as well. What this means is that when one starts from the equilibrium state (coiled state), the solution needs to experience a strain rate greater than a critical strain rate at least once to transition to the stretched state. However due to coil−stretch hysteresis, the stretched state can be sustained at strain rates lower than the critical strain rate after the polymer is stretched.[55] Since the simulations can be performed only for a finite strain, the number of chains hopped in a particular system is always

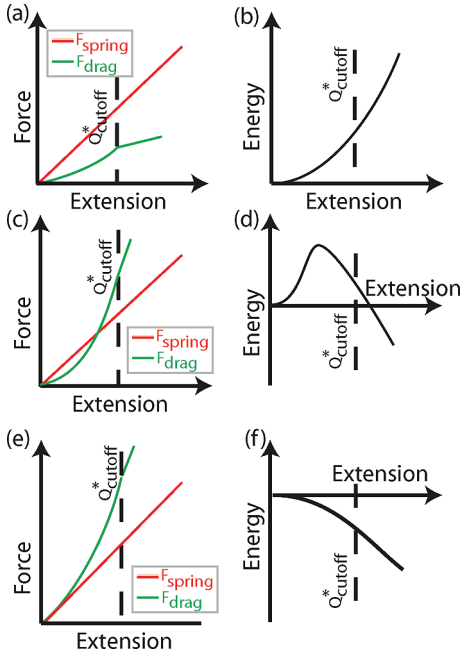

Figure 1. Force profiles and energy landscapes for a Hookean dumbbell at different strain rates. (a) At $Pe < Pe_{lower}$, forces intersect only at $Q^* = 0$ (stable point) (b) At $Pe < Pe_{lower}$, the energy minima occurs only at coiled state (c) At $Pe_{lower} < Pe < Pe_{upper}$, Forces intersect at $Q^* = 0$ and $Q^* < Q^*_{cutoff}$ (d) At $Pe_{lower} < Pe < Pe_{upper}$, an energy barrier exists with two minima (e) At $Pe > Pe_{upper}$, Forces intersect only at $Q^* = 0$ (unstable point) (f) At $Pe > Pe_{upper}$, the energy minima occurs only at stretched state while a maxima exists at coiled state ($Q^* = 0$).

underestimated from the true steady state at infinite strain. For eg., if 50% of chains hop at strain 200 at a fixed strain rate, then this strain rate may correspond to 100% chain hop at infinite strain. So a *Pe* number which reveals an energy barrier in finite strain simulations is expected to be closer to the Pe_{upper} at the true steady state. Hence we expect the scaling exponent of critical strain rate (Pe_c) from simulations to be $(1 + \nu)$. In principle, the dumbbell model parameters in good solvents can be found by performing rigorous multibead spring simulations following the already established methodology for Θ solvents.[22] However, incorporating solvent quality effects in dumbbell model is nontrivial since solvent quality affects both the equilibrium and nonequilibrium properties of the system thereby affecting both the conformation dependent drag as well as the equivalent spring force. Hence, we perform and analyze the rigorous multibead spring simulations directly to explore the solvent quality effects.

4. Relaxation Times

A basic characteristic of polymer solutions is their relaxation spectrum which determines all manifestations of their viscoelastic properties. The two most important relaxation times are the relaxation time based on the zero shear rate viscosity (which is the sum of all the relaxation times) and the longest relaxation time (which corresponds to the relaxation of the largest length scales of polymer). For a polymer with *m* relaxation modes, the relaxation time based on the zero shear rate viscosity λ_η is given by

$$\lambda_\eta = \lambda_1 + \lambda_2 + ... + \lambda_m \tag{21}$$

where λ_1 is the longest relaxation time. We have calculated the relaxation time based on the zero shear rate viscosity using the Green−Kubo autocorrelation formulation[54,56] from equilibrium simulations.[2] The longest relaxation time can be obtained by fitting a 3 parameter−exponential (A, λ_1^*, B) to the decay of a size measure of the polymer chain like the mean square end to end distance as follows:[21]

$$\langle Q^*_{e-e}{}^2 \rangle = Ae^{-t^*/\lambda_1^*} + B \tag{22}$$

where $Q^*_{e\text{-}e}{}^2$ is the square of the polymer end-to-end distance, and *B* is its value at equilibrium as shown in Figure 2. We perform simulations to calculate the relaxation times and nonequilibrium properties for a range of molecular weights: $N = 11, 12, 13, 14, ..., 24, 25$. The simulation time scales as $N^{2.25}$ and it grows very fast as *N* increases beyond 25. Moreover, the range 11−25 provides sufficient information to deduce the required results. Also we study a range of solvent qualities: $z = 0$ (Θ solvent), 1 (good solvent), 5 (better solvent), 10 (extremely good solvent). We choose $K = 1$, where $d^* = Kz^{*1/5}$ is the dimensionless range of the EV potential.

The longest relaxation time can also be calculated by fitting a decaying exponential to the tail of the near-equilibrium stress relaxation calculated using the Green Kubo autocorrelation. The ratio of the two relaxation times (λ_η^* and λ_1^*) is known to be independent of chain length *N* in Θ solvents in the limit of long chains.[38] Here, we find that this ratio is independent of chain length at any solvent quality (Figure 3) and hence a universal function of solvent quality.

$$\Gamma_{\eta,1} = \left.\frac{\lambda_\eta^*}{\lambda_1^*}\right|_{N\to\infty} \tag{23}$$

Remarkably, the effect of solvent quality is proportionally enhanced in both these relaxation times such that their ratio is independent of molecular weight and only a function of solvent quality. This finding provides a very useful means to experimentalists to calculate one relaxation time from the other without having to perform both the experiments separately. Since the universal function monotonically increases with solvent quality, one can infer that the solvent quality affects the lower relaxation modes more prominently than the longest relaxation mode.

5. Critical Strain Rate

The macroscopic properties of polymer solutions are a strong function of the conformation of the polymer (coiled or stretched state). When long chain, linear polymers in dilute solutions are subjected to purely elongational flows or elongation-dominated mixed flows, the solution properties vary drastically near a critical strain rate. This critical strain rate characterizes the coil−stretch transition of polymer conformation. It is important to distinguish the two different coil-stretch transitions affecting macroscopic properties at different time-scales (Figure 4).

1. When an equilibrated polymer chain is exposed to a strong extensional flow, the polymer takes some time to unravel to the stretched state. If the strain rate is above a critical strain rate, the polymer conformation undergoes a coil to stretch transition (CS-I) at some finite strain. The strain (of the fluid) is the product Pe*time. The value of strain at which the transition takes place (transition time) is a strong function of chain length and strain rate.[57] This transient coil−stretch transition (CS-I) is very sharp in elongational flows and gets sharper with increase in the molecular weight of the polymers. Molecular individualism, residence time before transition, conformational shape evolution etc are important aspects of this transition.[58,59] This transition reflects the transient properties of the polymeric solution.
2. One can also consider the conformational variation of a polymer at a fixed strain when exposed to different

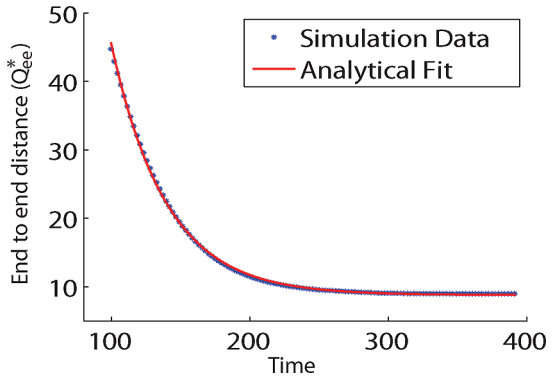

Figure 2. Longest relaxation time for Hookean chains with $N = 14$, $z = 5$. A three-parameter exponential is fit to the tail of the decaying function of the end-to-end extension of the chain as a function of time to calculate the longest relaxation time λ_1^*.

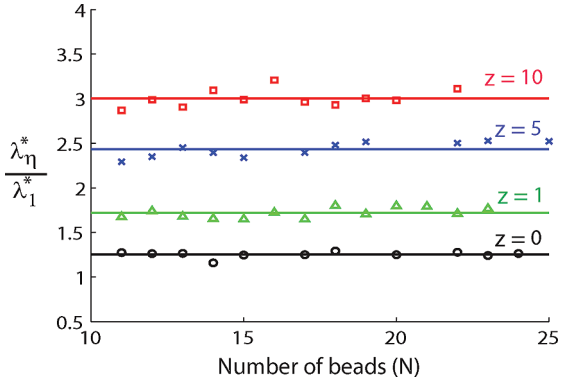

Figure 3. Ratio of the two relaxation times: relaxation time based on the zero shear rate viscosity (λ^*_η) and longest relaxation time (λ_1^*) for Hookean chains. The ratio is independent of molecular weight and only a function of solvent quality.

strain rates. It is observed that there is again a transition from coiled state to stretched state near a particular strain rate. Each point on this coil−stretch transition (CS-II) (at a fixed strain) is a result of a different transient experiment. At infinite strain, this coil stretch transition (CS-II) is very sharp for extensional flows and reflects the steady state properties of the polymer solutions.

In short, CS-I is a function of strain at a fixed strain rate while CS-II is a function of strain rate at a fixed strain. In other words, in CS-I, Pe = constant as time increases while in CS-II, Pe* time = constant and experiments with smaller Pe imply longer times (and vice versa). It is important to note that the critical strain rate beyond which CS-I occurs and the critical strain rate for CS-II transition of steady state properties (CS-II at infinite strain) is the same.

Since the solution properties change dramatically at this so-called coil−stretch transition (CS-I or CS-II), it is important in many applications. This transition is primarily characterized by the critical strain rate

$$Pe_c = \lambda_H \dot{\varepsilon}_c$$

for a given polymer molecular weight and solvent quality. A hop is physically defined as the coil to stretch transition and a more appropriate mathematical definition is given later. As discussed earlier, no chain hops at strain rates below Pe_{lower} while all chains hop at strain rates above Pe_{upper}. Since simulations and experiments can be performed only for a finite strain, the number of

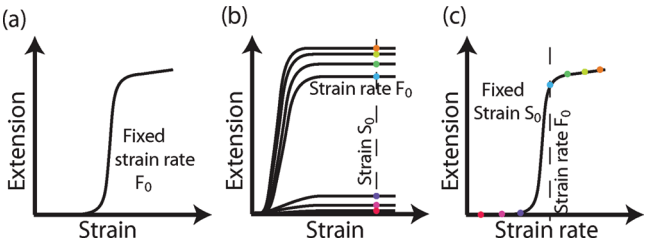

Figure 4. Coil−stretch transitions (a) Illustrates CS-I at a fixed strain rate (F_0) (b) Illustrates how one gets CS-II at a fixed strain from multiple CS-I at different strain rates (c) Illustrates CS-II at a fixed strain (S_0).

chains hopped is always underestimated in simulations relative to that at the true steady state. Hence, the critical strain rate (Pe_c) that we obtain from simulations is a better approximation of Pe_{upper} rather than Pe_{lower}.

We approach this problem of estimating the critical strain rate by three different strategies. In one approach, we simulate a single chain for a very long strain (5000 to practically infinite strain for any physical system). It is referred to as the SCLS (single chain long strain) approach in this article. In the second approach, we take an ensemble of chains ($N_{\text{ensemble}} = 1000$) and study their kinetics for a long strain (200−300 to practically infinite strain for any experiment). This approach is referred to as THOP as it is primarily based on computing mean hop times. The third approach also uses an ensemble of chains ($N_{\text{ensemble}} = 1000$) and is based on counting the number of chains that hop (NHOP).

In the first approach (SCLS), a polymer chain is first equilibrated for approximately 10 relaxation times under no-flow conditions. The extensional flow is then switched on and the end-to-end distance (which is a good indicator of macroscopic properties of the solution) of the chain is observed for a very large strain of 5000. A chain is considered to have 'hopped' to the stretched state if the end-to-end extension of the chain reaches beyond $Q^*_{\text{cutoff}} = 10^4 Q^*_{\text{eqm}}$ where Q^*_{eqm} is the equilibrium extension of the chain under no-flow conditions. To avoid counting huge conformational fluctuations of Hookean chains as they hop, it is ensured that the extension is sustained above the cutoff value (Q^*_{cutoff}) for at least one relaxation time. To save computational time, the chain is discarded after it hops since we are concerned only with the critical strain rate for coil stretch transition in this study.

Coil stretch transitions CS-I are obtained by recording the end to end distance as a function of strain at a fixed solvent quality and strain rate as shown in Figure 5 for $N = 14$. Clearly, the coil stretch transitions (CS-I) are very sharp in extensional flows. As the solvent quality improves at a fixed strain rate, the chains unravel faster (at a lower strain) as shown in Figure 5a. Also as the strain rate increases at a fixed solvent quality ($z = 1$), the chains take less time to hop (Figure 5b). Thus, we find that the transient properties (CS-I) are a function of both strain rate and solvent quality. This can be attributed to the swollen equilibrium state of the polymer due to more favorable interactions between polymer and solvent molecules with improvement in solvent quality. CS-II can be computed using the data collected as described above for different strain rates. For this, the magnitude of end to end extension of the polymer at a fixed strain (= 5000) from different simulation runs (at different strain rates) is plotted as a function of strain rates as shown in Figure 6. Using these curves, we computed the critical strain rates below which the chain never hops and above which the chain always hops. It is observed that the difference in the two critical strain rates is of the order of 10^{-4}. Moreover, despite the fact that the strain (5000) is very large, it is still a finite strain and there is always a nonzero probability of a chain that has not hopped at a strain 5000 will hop at a later strain (e.g., 10000). Hence, the critical strain rate

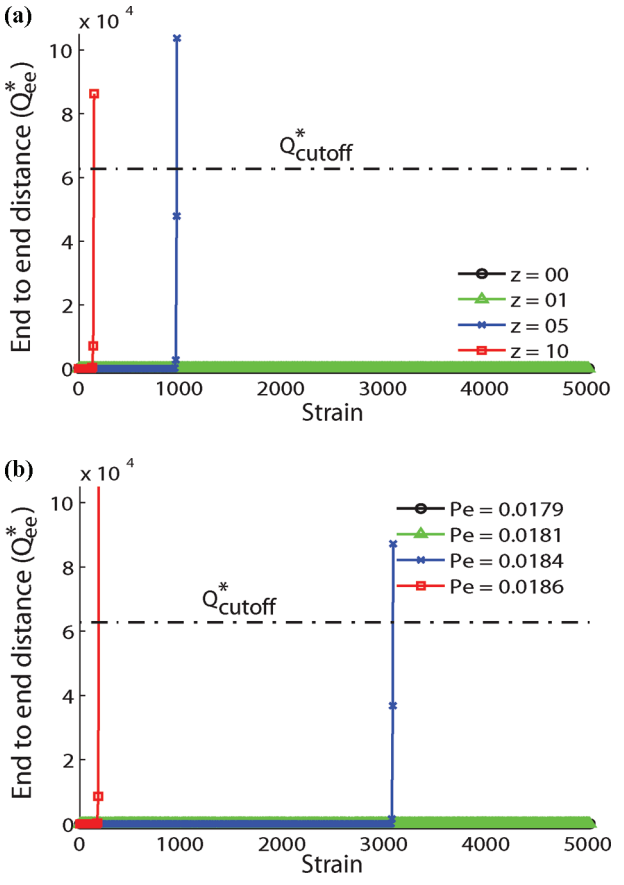

Figure 5. Simulation results for CS-I by single chain simulation (SCLS) approach ($N = 14$): (a) CS-I transitions again occur at a lower strain (faster) as the solvent quality improves at a fixed strain rate ($Pe = 0.018$); (b) CS-I transitions occur at a lower strain (faster) as the strain rate increases at a fixed solvent quality ($z = 1$).

that we get from these simulation results is expected to be greater than Pe_{lower} and a closer approximation of Pe_{upper}. The effect of solvent quality can be clearly seen on CS-II at strain 5000 wherein the critical strain rate decreases with improvement in solvent quality (Figure 6). We compute the critical strain rate using this approach for a range of molecular weights ($N = 11, 12, 13, ..., 25$) and solvent qualities ($z = 0, 1, 5, 10$) and the results for ($N = 14$, $z = 0, 1, 5, 10$) are reported in Table 1.

In the second approach (THOP), we explore the kinetics of an ensemble of 1000 chains (Figure 7). For this, the mean time taken by a chain in the ensemble to hop is measured.

$$\text{mean hop time} = \left(\sum_{i=1}^{N_{\text{ensemble}}} t_i^{\text{hop}}\right)/N_{\text{ensemble}} \qquad (24)$$

where t_i^{hop} is the time taken by chain i to hop starting from the equilibrium state. It is observed that as the strain rate decreases, it takes longer for chains to hop and hence the mean hop time increases. The mean hop time diverges at the critical strain rate since the chains do not hop below a critical strain rate even if one waits for infinite time. This critical strain rate can be found using the extrapolation technique as shown in Figure 7. The divergence of the mean hop time gets sharper as the solvent quality improves. Certainly for $Pe < Pe_{\text{lower}}$, the mean hop time is infinite since none of the chains hop. However, even for strain rate (Pe) such that ($Pe_{\text{lower}} < Pe < Pe_{\text{upper}}$), the mean hop time is infinite since this is the case if even one chain in the ensemble does not hop. Hence the critical strain rate Pe_c obtained from this approach is also a better approximation of Pe_{upper} than Pe_{lower}. The critical

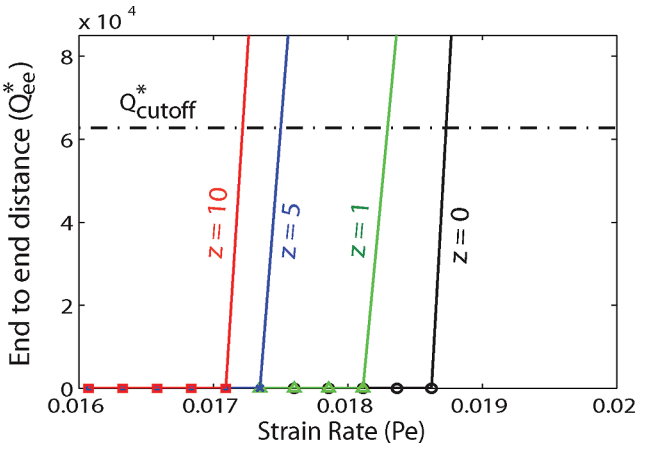

Figure 6. Simulation results for CS-II at fixed strain (=5000) by single chain simulation (SCLS) approach ($N = 14$) for different solvent qualities. The critical strain rate decreases as the solvent quality improves.

Table 1. Critical Strain Rate (Pe_c) for $N = 14$

z	Pe_c (NHOP)	Pe_c (THOP)	Pe_c (SCLS)
0	0.0199	0.0194	0.0186
1	0.0189	0.0185	0.0181
5	0.0182	0.0179	0.0174
10	0.0177	0.0172	0.0171

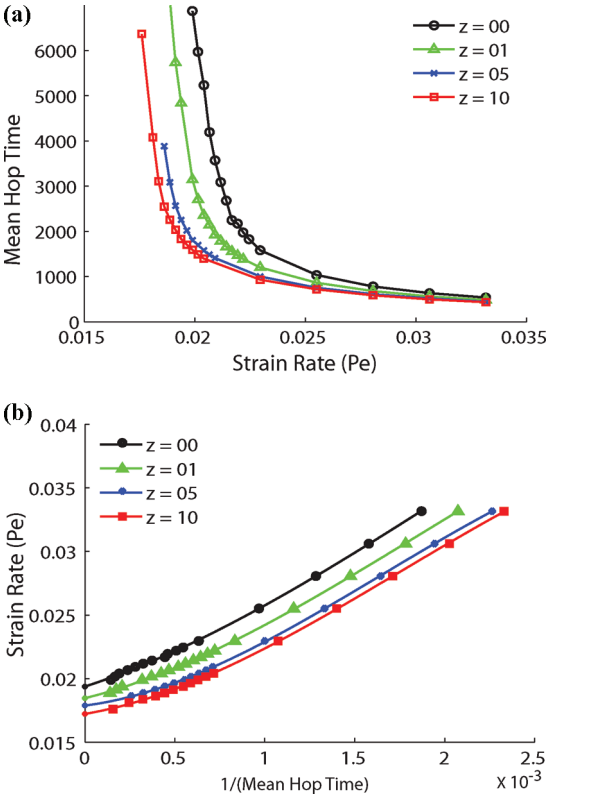

Figure 7. Simulation results using THOP approach for mean hop time for an ensemble of Hookean chains ($N = 14$): (a) mean hop time increases as the strain rate decreases and the increase is faster as the solvent quality improves. (b) extrapolation of mean hop time to infinity corresponding to the critical strain rate. Critical strain rate decreases with improvement in solvent quality.

strain rate is found to decrease as the molecular weight increases and/or as the solvent quality improves consistent with the predictions by our SCLS approach discussed earlier. We compute

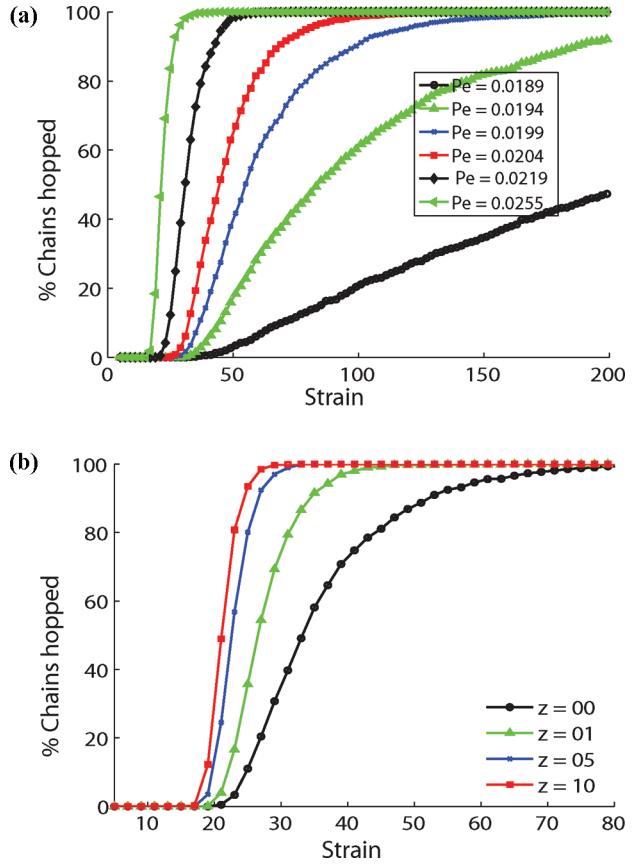

Figure 8. Simulation results for CS-I using the NHOP approach for Hookean chains ($N = 14$). (a) At fixed solvent quality ($z = 1$), CS-I gets sharper with increase in strain rate and occurs at lower values of strain. (b) CS-I gets sharper and faster with improvement in solvent quality at any fixed strain rate ($Pe = 0.023$).

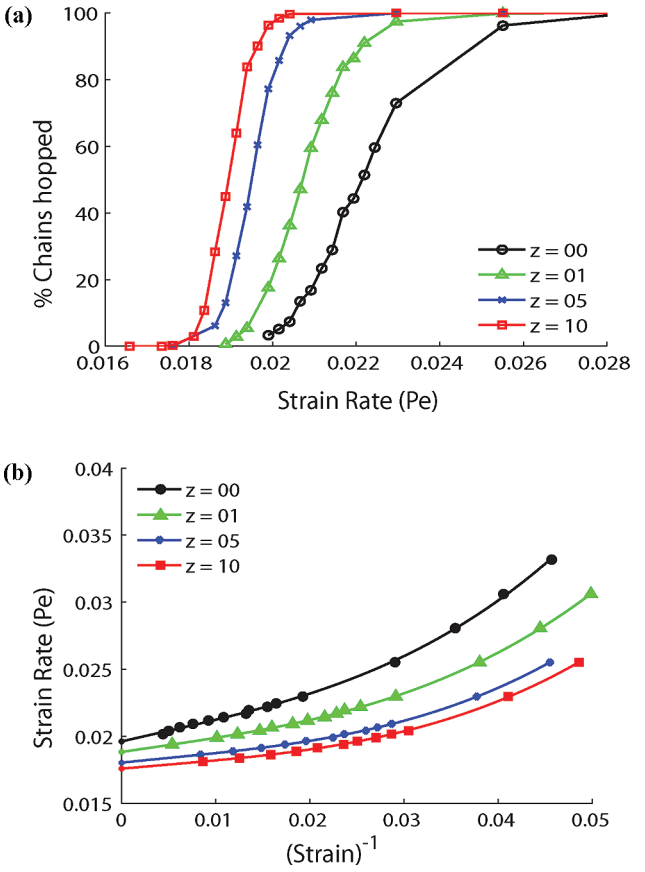

Figure 9. Simulation results for CS-II using the NHOP approach for Hookean chains ($N = 14$). (a) CS-II at fixed strain ($=40$) gets sharper with improvement in solvent quality. (b) Critical strain rate can be calculated by extrapolating finite simulation results at a fixed percentage of chains hopped ($= 90\%$) to strain $\rightarrow \infty$. The critical strain rate decreases as the solvent quality improves.

the critical strain rate using this approach for a range of molecular weights ($N = 11, 12, 13, ..., 25$) and solvent qualities ($z = 0, 1, 5, 10$) and the results for ($N = 14$, $z = 0, 1, 5, 10$) are reported in Table 1.

For Hookean chains, since a single chain can have essentially infinite extension, all average properties become unbounded in an ensemble of chains past a critical strain rate. At a given strain rate and strain on the other hand, we can examine the percentage of chains that have hopped. Thus, we explore the evolution of the probability distribution of the chains (hopped or unhopped) as a function of strain at different strain rates. The probability distribution evolves from unimodal (at coiled state) to bimodal (hysteretic regime) to unimodal (at stretched state) as the strain rate increases as shown in Figure 1. We find that an increasing percentage of chains hop at any strain as the strain rate increases (Figure 8 and Figure 9). Also as the strain rate increases, the chains hop at lower values of strain. Moreover, all the chains hop within an increasingly narrow range of strain as the strain rate increases leading to sharper CS-I (Figure 8). We also find that solvent quality significantly affects the transient properties (CS-I) since a greater percentage of chains hop at any strain for a fixed strain rate as the solvent quality improves. These observations for the percentage number of chains hopped (NHOP) resonate with the conclusions from the earlier approaches (SCLS and THOP). We can also examine the effect of solvent quality on CS-II at a strain of 40 for this ensemble of chains (Figure 9) and find that the critical strain rate seems to decrease. To get more accurate results for steady state, we extrapolate the finite strain simulation results to infinite strain as shown in Figure 9. Note that the extrapolated results are obtained at infinite strain based on the finite strain data for 90% chain hops. Hence the critical strain rate obtained from this approach is also larger than Pe_{lower} and hence a closer approximation to Pe_{upper}. This analysis is repeated for a wide range of molecular weights ($N = 11, 12, 13, ..., 25$) and solvent quality ($z = 0,1,5,10$). Apart from the qualitative agreement of the coil stretch transitions (both CS-1 and CS-II) between the three approaches (SCLS, THOP, and NHOP), the numerical value of the critical strain rates are also in remarkable agreement (see Table 1 for values corresponding to all three methods for $N = 14$ for various values of z).

6. Scaling Exponent and Universal Functions

It is important to note that the polymer properties follow power law behavior only in Θ solvents or extremely good solvents. In the crossover region in between, the polymer properties are simply a function of the solvent quality parameter z.[46,60] However, one can extract an effective scaling exponent for the properties in the crossover region at a fixed solvent quality (z) as shown in Figure 10. The effective scaling exponent is found to be a function of solvent quality for both relaxation times as well as the critical strain rate. The results for different solution properties are reported for a range of solvent qualities in Table 2.

One can define two different critical Deborah numbers that can be used to characterize flows based on the two different relaxation times:

$$De_1 = Pe_c\lambda_1^*$$

$$De_\eta = Pe_c\lambda_\eta^*$$

Since the relaxation times increase while the critical strain rates decrease with solvent quality, the effect of solvent quality on the product (Deborah number) needs further analysis. Interestingly, we find that both the critical Deborah numbers (De_1 and De_η) are independent of molecular weight. However their response to solvent quality is different. De_1 is found to be independent of solvent quality while De_η increases with improvement in solvent quality (see Figure 11).

In the crossover region, we compute the universal dependence of relaxation times and critical strain rates on solvent quality by analyzing their behavior in the infinite chain length limit. It is well-known that the temperature and molecular weight dependence of any macroscopic property ϕ under good solvent conditions (for various polymer−solvent systems, molecular weights and temperatures) can be collapsed onto a master curve given by[41]

$$\phi = \phi_\theta U_\phi(z) \tag{25}$$

where ϕ_θ is the value of the same property under Θ conditions and $U_\phi(z)$ is a universal function of z. One can define universal properties for the relaxation times and critical strain rates as follows:

$$U_\eta = \left.\frac{\lambda_\eta^*(z)}{\lambda_{\eta,\theta}^*}\right|_{N\to\infty} \qquad U_1 = \left.\frac{\lambda_1^*(z)}{\lambda_{1,\theta}^*}\right|_{N\to\infty} \qquad U_{Pe} = \left.\frac{Pe_c(z)}{Pe_{c,\theta}}\right|_{N\to\infty} \tag{26}$$

The universal function is obtained by the extrapolation of finite bead number simulation results to the infinite bead number limit keeping the solvent quality fixed (see Figure 12 for $z = 5$). The variation of these universal properties with z is shown in Figure 13. Each point on this curve is obtained by extrapolating the ratio at finite bead number to the infinite bead number limit. As the solvent quality improves, the value of U_η increases. This suggests that the relaxation process is slowed down with improving solvent quality. As the solvent quality improves, U_1 also increases though this increase is not as pronounced as in the universal function based on the zero shear rate viscosity U_η. However, U_{Pe} decreases as the solvent quality improves. This is because the polymer chains are swollen in good solvents and hence the initial strain rate required to initiate coil stretch transition is lower in good solvents.

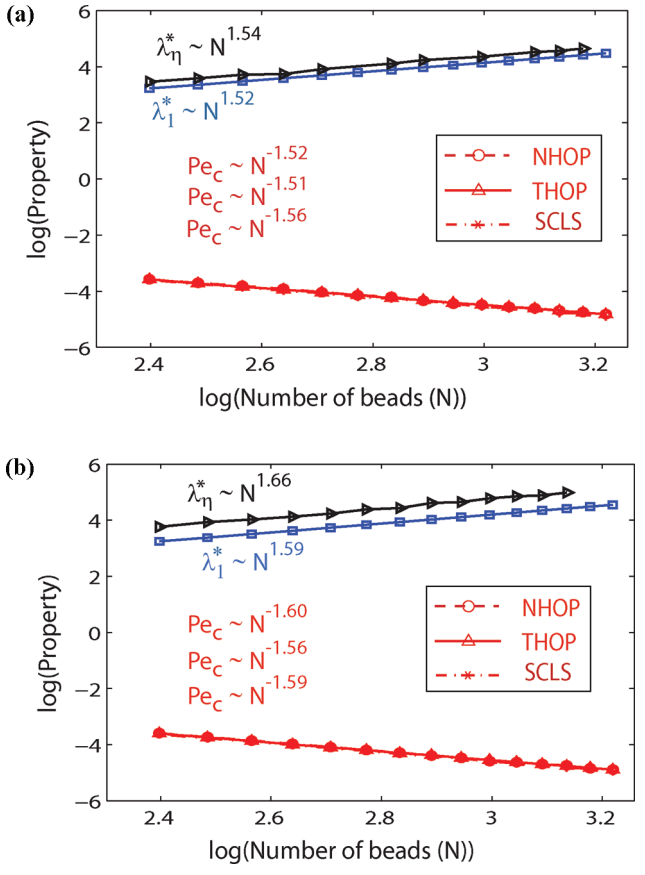

Figure 10. Simulation results for scaling exponents with molecular weight (m:$P = cN^m$) for relaxation times (λ_1^* and λ_η^*) and critical strain rate (Pe_c) calculated by three different approaches (SCLS, NHOP and THOP) at (a) $z = 0$ and (b) $z = 1$.

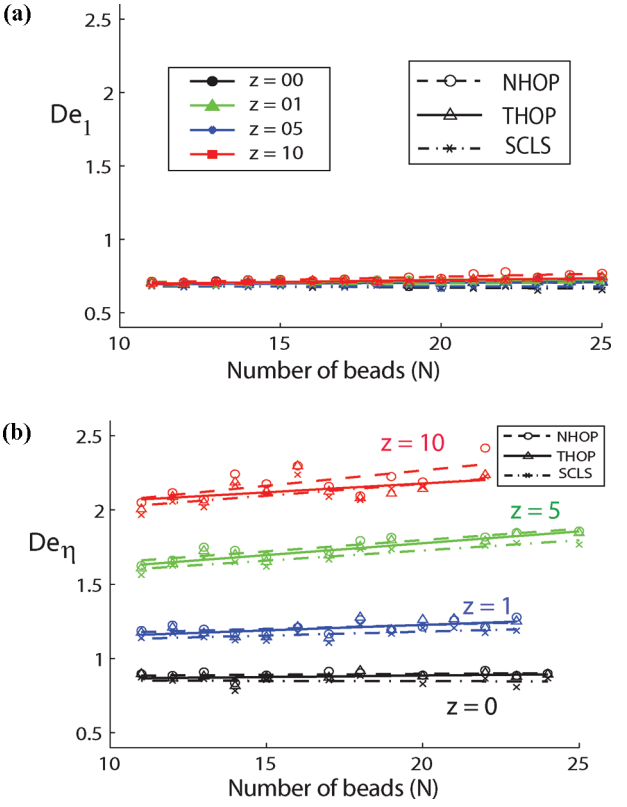

Figure 11. (a) Deborah number De_1 is independent of molecular weight as well as solvent quality. The critical strain rate is calculated by 3 different methods (SCLS (dashed line), THOP (solid line) and NHOP (dash-dotted line)). (b) De_η is independent of molecular weight, however it increases with improvement in solvent quality. Again the critical strain rate is calculated by three different methods (SCLS, THOP, and NHOP).

Table 2. Scaling Exponents m: Property = N^m

property	power law relation	$m(z = 0)$	$m(z = 1)$	$m(z = 5)$	$m(z = 10)$
critical strain rate (NHOP)	$Pe_c = cN^m$	−1.52	−1.60	−1.64	−1.64
critical strain rate (THOP)	$Pe_c = cN^m$	−1.51	−1.56	−1.64	−1.67
critical strain rate (SCLS)	$Pe_c = cN^m$	−1.56	−1.59	−1.65	−1.66
longest relaxation time	$\lambda_1^* = cN^m$	1.52	1.59	1.68	1.73
zero shear rate viscosity	$\lambda_\eta^* = cN^m$	1.54	1.66	1.79	1.79

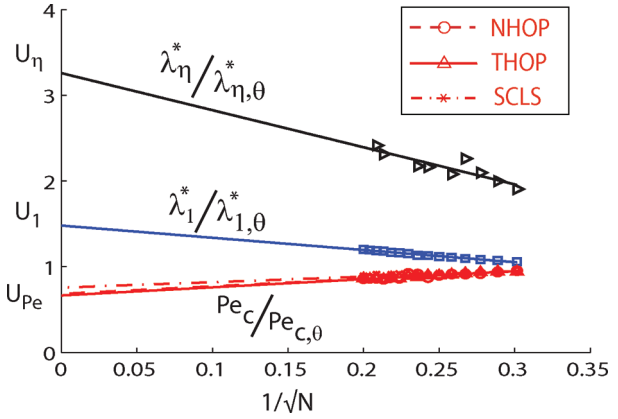

Figure 12. Extrapolation of the ratio of Pe_c, λ_1^* and λ_η^* at $z = 5$ to their Θ-solvent values to the $N \rightarrow \infty$ limit. The relaxation times increase while the critical strain rates decrease with improvement in solvent quality. The critical strain rates are calculated by 3 different approaches (SCLS, THOP and NHOP).

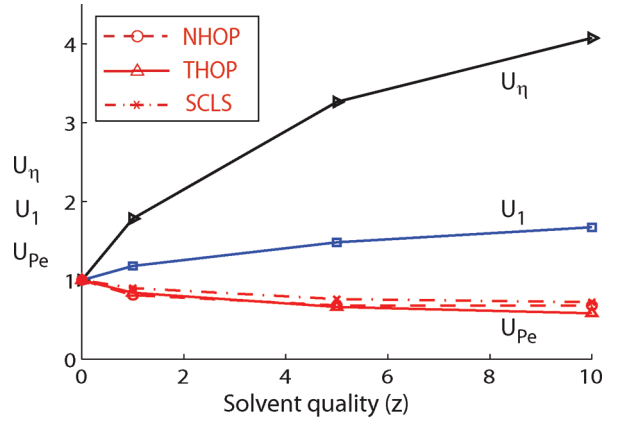

Figure 13. Universal functions for the ratio of (a) longest relaxation time (λ_1^*), relaxation time based on the zero shear rate viscosity (λ_η^*) and critical strain rate (Pe_c) to their Θ-solvent values as a function of solvent quality. The critical strain rate decreases while the relaxation times increase with improvement in solvent quality.

One can also find the universal functions based on the Deborah numbers defined earlier. We can compute the universal number based on De_1 by two different methods as indicated in the equations below

$$\text{method A}: \quad U_{De}^1 = \left.\frac{De_1(z)}{De_{1,\theta}}\right|_{N\rightarrow\infty} = \left.\frac{Pe_c(z)\lambda_1^*(z)}{Pe_{c,\theta}\lambda_{1,\theta}^*}\right|_{N\rightarrow\infty} \tag{27}$$

$$\text{method B}: \quad U_{De}^1 = \left.\frac{Pe_c(z)}{Pe_{c,\theta}}\right|_{N\rightarrow\infty} \left.\frac{\lambda_1^*(z)}{\lambda_{1,\theta}^*}\right|_{N\rightarrow\infty} = U_{Pe}U_1 \tag{28}$$

In method A, it is found as an extrapolation limit of the ratio of Deborah numbers (good solvent to Θ solvent) at each bead number. In method B, it is found as a product of two extrapolation limits for the ratio of critical strain rate and the ratio of longest relaxation times at each bead number. The results with the different methods match quite closely as shown in Figure 14a. It is observed that as the solvent quality improves, U_{De}^1 remains close to one i.e. the magnitude of U_{De}^1 in a good solvent is the same as that in Θ solvent. This is because the decrease in critical strain rate is compensated by the increase in relaxation time λ_1^* as solvent quality improves.

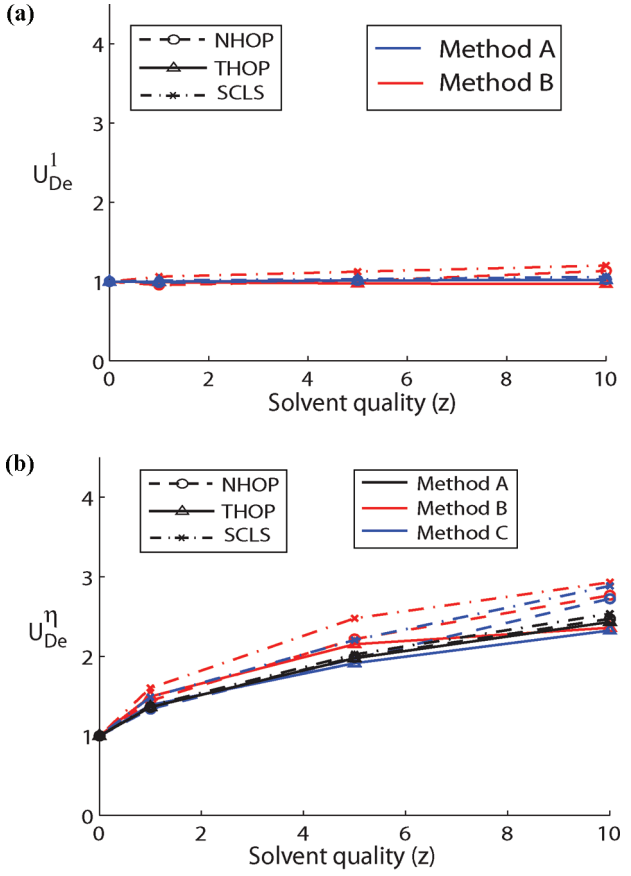

Figure 14. (a) Universal function for the ratio of De_1 to its Θ-solvent value as a function of solvent quality. (b) Universal function for the ratio of De_η to its Θ-solvent value as a function of solvent quality. De_1 is independent of solvent quality while De_η increases as the solvent quality improves.

On similar lines, the universal number based on De_η can be obtained by three different methods as shown by the equations below:

$$\text{method A}: \quad U_{De}^\eta = \left.\frac{De_\eta(z)}{De_{\eta,\theta}}\right|_{N\rightarrow\infty} = \left.\frac{Pe_c(z)\lambda_\eta^*(z)}{Pe_{c,\theta}\lambda_{\eta,\theta}^*}\right|_{N\rightarrow\infty} \tag{29}$$

$$\text{method B}: \quad U_{De}^\eta = \left.\frac{Pe_c(z)}{Pe_{c,\theta}}\right|_{N\rightarrow\infty} \left.\frac{\lambda_\eta^*(z)}{\lambda_{\eta,\theta}^*}\right|_{N\rightarrow\infty} = U_{Pe}U_\eta \tag{30}$$

$$\text{method C}: \quad U_{De}^\eta = U_\eta U_{Pe} = \left(\frac{\Gamma_{\eta,1}(z)}{\Gamma_{\eta,1,\theta}}U_1\right)U_{Pe} = \frac{\Gamma_{\eta,1}(z)}{\Gamma_{\eta,1,\theta}}U_{De}^1 \tag{31}$$

In method A, the universal number U_{De}^η is found as an extrapolation limit of the ratio of Deborah numbers (good solvent to Θ solvent) at each bead number. In method B, it is found as a product of two extrapolation limits for the ratio of critical strain rate and the ratio of relaxation times based on zero shear rate viscosity at each bead number. In method C, it is obtained as product of three extrapolation limits: (a) the ratio of the good solvent to Θ-solvent value of the ratio of two relaxation times $[\Gamma_{\eta,1}(z)/\Gamma_{\eta,1}|(\Theta)]$ (see eq 23), (b) the ratio of the good solvent to Θ-solvent value of the longest relaxation times, and

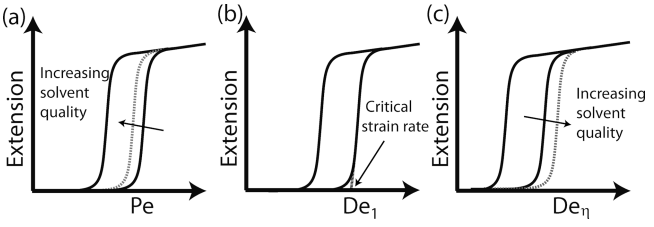

Figure 15. Effect of solvent quality on the width of conformational hysteresis.

(c) the ratio of the good solvent to Θ-solvent value of the critical strain rate at each bead number.

Unlike U^1_{De}, U^η_{De} increases with improvement in solvent quality. This can be attributed to a greater increase in relaxation time λ^*_η as compared to the decrease in critical strain rate. Thus, we see that the critical Deborah number based on the longest relaxation time remains a constant independent of the solvent quality while the one based on the zero shear rate viscosity is a different constant for different solvent qualities. Accordingly, depending on the flow characterization (Pe or De_1 or De_η), the coil-to-stretch arm of hysteresis remains unaffected or shifts leftward or rightward. The stretch-to-coil arm of hysteresis is unaffected by solvent quality as the EV effects are negligible in the stretched state. Hence the width of hysteresis remains invariant or increases or decreases as shown in Figure 15 depending on the flow characterization.

7. Conclusions

Brownian dynamics simulations are used to study the coil stretch transition of dilute polymer systems. Two different relaxation times (λ_1 and λ_η) are evaluated. The critical strain rate is computed by three different approaches based on very different aspects of polymer dynamics: SCLS (single chain simulations for strain 5000), THOP (kinetic analysis by computing mean hop time for an ensemble of 1000 chains) and NHOP (probability distribution analysis by counting number of chains hopped at any given strain). Extrapolation techniques are used to obtain steady state results from finite strain simulations specifically in the THOP and NHOP approaches. The results from all the approaches agree both qualitatively as well as quantitatively. The solvent quality is found to affect both the transient and steady state properties significantly. As the solvent quality improves, the chains unravel faster and the onset of coil stretch transition occurs at lower strains. The critical strain rate decreases and the coil stretch transitions (both CS-I and CS-II) get sharper as the solvent quality improves. The magnitude of the scaling exponent of the critical strain rate with molecular weight increases with improving solvent quality and is in agreement with the 1-D conformational energy theory for dumbbell model. Deborah numbers (De_1 and De_η) and the ratio of two relaxation times ($\Gamma_{\eta,1}$) are found to be independent of molecular weight. Interestingly, the critical Deborah number based on the longest relaxation time (De_1) is found to be independent of solvent quality while the critical Deborah number based on the zero shear rate viscosity (De_η) is a monotonically increasing function of solvent quality. We have also explored the universal behavior of these properties by extrapolating to the infinite chain length limit. Specifically we find U_η, U_1, U_{Pe}, U^1_{De}, U^η_{De}, and $\Gamma_{\eta,1}$ as universal functions of solvent qualities.

Acknowledgment. This work was supported by the Australian Research Council (ARC) under the Discovery Projects program and by the National Science Foundation under Grant CTS-0522564. In addition, an international linkage grant from the ARC enabled Shikha Somani to spend several extended stays at Monash University, and facilitated the collaboration between JRP and ESGS. All of this financial support is gratefully acknowledged. Computational resources were provided by the Australian Partnership for Advanced Computation (APAC), and the Monash Sun Grid Cluster. The authors thank Steve Jones at Stanford and Philip Chan and Wojtek Goscinski at Monash for their help in making additional computational resources available. Finally, the authors also thank Dr Jaroslaw Bosko and Dr. R. Prabhakar for very insightful discussions.

References and Notes

(1) Schroeder, C.; Babcock, H.; Shaqfeh, E.; Chu, S. *Science* **2003**, *301*, 1515.
(2) Prabhakar, R.; Prakash, J. *J. Non-Newtonian Fluid Mech.* **2004**, *116*, 163–182.
(3) Prabhakar, R.; Prakash, J. *J. Rheol.* **2002**, *46*, 1191.
(4) De Gennes, P. G. *J. Chem. Phys.* **1974**, *60*, 5030.
(5) Hinch, E. *Phys. Fluids* **1977**, *20*, S22.
(6) Tanner, R. *J. Rheol.* **1975**, *19*, 557.
(7) Fan, X.; Byron Bird Michael, R. *J. Non-Newtonian Fluid Mech.* **1985**, *18*, 255–272.
(8) Wiest, J.; Wedgewood, L.; Bird, R. *J. Chem. Phys.* **1989**, *90*, 587.
(9) Liu, T. W. *J. Chem. Phys.* **1989**, *90*, 5826.
(10) Darinskii, A.; Lyulin, A.; Saphiannikova, M. *Int. J. Polym. Mater.* **1993**, *22*, 15–24.
(11) Brestkin, Y. *Acta Polym.* **1987**, *38*, 470–477.
(12) Magda, J.; Larson, R.; Mackay, M. *J. Chem. Phys.* **1988**, *89*, 2504.
(13) Rallison, J.; Hinch, E. *J. Non-Newtonian Fluid Mech.* **1988**, *29*, 37–55.
(14) Keller, A.; Odell, J. *Colloid Polym. Sci.* **1985**, *263*, 181–201.
(15) Harlen, O.; Hinch, E.; Rallison, J. *J. Non-Newtonian Fluid Mech.* **1992**, *44*, 229–265.
(16) Sridhar, T.; Nguyen, D.; Prabhakar, R.; Prakash, J. *Phys. Rev. Lett.* **2007**, *98*, 167801.
(17) Celani, A.; Puliafito, A.; Vincenzi, D. *Phys. Rev. Lett.* **2006**, *97*, 118301.
(18) Gerashchenko, S.; Steinberg, V. *Phys. Rev. E* **2008**, *78*, 40801.
(19) Prakash, J. *Kor.-Austr. Rheol. J.* **2009**, *21*, 245–268.
(20) Hsieh, C.; Larson, R. *J. Rheol.* **2005**, *49*, 1081.
(21) Schroeder, C.; Shaqfeh, E.; Chu, S. *Macromolecules* **2004**, *37*, 9242–9256.
(22) Beck, V.; et al. *J. Chem. Phys.* **2008**, *124*, 094902.
(23) Hoffman, B.; Shaqfeh, E. *Phys. Rev. E* **2008**, *78*, 55301.
(24) Cathey, C.; Fuller, G. *J. Non-Newtonian Fluid Mech.* **1990**, *34*, 63–88.
(25) Menasveta, M.; Hoagland, D. *Macromolecules* **1992**, *25*, 7060–7062.
(26) Narh, K.; Odell, J.; Keller, A. *J. Polym. Sci., Part B: Polym. Phys.* **1992**, *30*, 335–340.
(27) Farrell, C.; Keller, A.; Miles, M.; Pope, D. *Polymer* **1980**, *21*, 1292–1294.
(28) Frank, F. C.; K., A.; R., M. M. *Polymer* **1971**, *12*, 467.
(29) Nguyen, Q.; Kausch, H. *Flexible Polymer Chain Dynamics in Elongational Flow: Theory and Experiment*; Springer: Germany: 1999.
(30) Brestkin, Y.; Saddlkov, I.; Agranova, S.; Baranov, V.; Frenkel, S. *Polym. Bull.* **1986**, *15*, 147–151.
(31) Nguyen, T.; Yu, G.; Kausch, H. *Macromolecules* **1995**, *28*, 4851–4860.
(32) Rabin, Y.; Henyey, F.; Pathria, R. *Phys. Rev. Lett.* **1985**, *55*, 201–203.
(33) Mansfield, M.; Rakesh, L. *Polym. Commun.* **1989**, *30*, 327–329.
(34) Andrews, N.; Doufas, A.; McHugh, A. *Macromolecules* **1998**, *31*, 3104–3108.
(35) Cifre, J.; de la Torre, J. *J. Rheol.* **1999**, *43*, 339.
(36) Rabin, Y.; Öttinger, H. *Europhys. Lett.* **1990**, *13*, 423.
(37) Chen, J.; Kim, A. *Adv. Colloid Interface Sci.* **2004**, *112*, 159–173.
(38) Öttinger, H. *Stochastic processes in polymeric fluids*; Springer: Berlin: 1996.
(39) Bird, R. B.; Curtis, C. A. R.; Hassager, O. *Dynamics of polymeric liquids*; John Wiley: New York: 1987; Vol. *2*.
(40) Sunthar, P.; Prakash, J. *ANZIAM J.* **2004**, *46*, C320–C335.
(41) Sunthar, P.; Prakash, J. *Macromolecules* **2005**, *38*, 617–640.
(42) Somasi, M.; Khomami, B.; Woo, N.; Hur, J.; Shaqfeh, E. *J. Non-Newtonian Fluid Mech.* **2002**, *108*, 227–255.
(43) Schroeder, C.; Teixeira, R.; Shaqfeh, E.; Chu, S. *Macromolecules* **2005**, *38*, 1967–1978.

(44) Prabhakar, R.; Prakash, J.; Sridhar, T. *J. Rheol.* **2006**, *50*, 925.
(45) Prakash, J.; Ottinger, H. *Macromolecules* **1999**, *32*, 2028–2043.
(46) Kumar, K.; Prakash, J. *Macromolecules* **2003**, *36*, 7842–7856.
(47) Kumar, K.; Prakash, J. *J. Chem. Phys.* **2004**, *121*, 3886.
(48) Sunthar, P.; Nguyen, D.; Dubbelboer, R.; Prakash, J.; Sridhar, T. *Macromolecules* **2005**, *38*, 10200–10209.
(49) Sunthar, P.; Prakash, J. *Europhys. Lett.* **2006**, *75*, 77–83.
(50) Prakash, J. *J. Rheol.* **2002**, *46*, 1353.
(51) Graessley, W.; Hayward, R.; Grest, G. *Macromolecules* **1999**, *32*, 3510–3517.
(52) Hayward, R.; Graessley, W. *Macromolecules* **1999**, *32*, 3502–3509.
(53) Rubinstein, M.; Colby, R. H. *Polymer physics*; Oxford University Press: London, 2003.
(54) Doi, M.; Edwards, S. *The theory of polymer dynamics*; Oxford University Press: New York, 1988.
(55) Cifre, J.; de la Torre, J. *J. Non-Cryst. Solids* **1998**, *235*, 717–722.
(56) Fixman, M. *Macromolecules* **1981**, *14*, 1710–1717.
(57) Cifre, J.; de la Torre, J. *J. Chem. Phys.* **2001**, *115*, 9578.
(58) Perkins, T.; Smith, D.; Chu, S. *Science* **1997**, *276*, 2016.
(59) Hinch, E. *J. Non-Newtonian Fluid Mech.* **1994**, *54*, 209–230.
(60) Schäfer, L. *Excluded volume effects in polymer solutions, as explained by the renormalization group*; Springer Verlag: Berlin, 1999.